Title

Mechanically patterned neuromuscular junctions-in-a-dish have improved functional maturation

Journal

Molecular Biology of the Cell, 28(14)

ISSN

1059-1524

Authors

Happe, Cassandra L
Tenerelli, Kevin P
Gromova, Anastasia K
et al.

Publication Date

2017-07-07

DOI

10.1091/mbc.e17-01-0046

Peer reviewed

Mechanically Patterned Neuromuscular Junctions-in-a-dish Have Improved Functional Maturation

Cassandra L. Happe,[1] Kevin P. Tenerelli,[1] Anastasia K. Gromova,[2] Frederic Kolb,[1^] and Adam J. Engler[1-3*]

[1]Department of Bioengineering, University of California, San Diego, La Jolla, CA 92093, USA
[2]Biomedical Sciences Program, University of California, San Diego, La Jolla, CA 92093, USA
[3]Sanford Consortium for Regenerative Medicine, San Diego, La Jolla, CA 92037, USA
^Current Affiliation: Institut Gustave Roussy, Villejuif, France
*_Correspondence_: UC San Diego
9500 Gilman Drive / MC 0695
La Jolla, CA 92093
aengler@ucsd.edu
Phone: 858-246-0678
Fax: 858-534-5722

MANUSCRIPT INFORMATION

Running Title: Neuromuscular Junctions-in-a-dish
Keywords: Hydrogels, Stiffness,
Character Count: 25,119 (including spaces but excluding references, figure legends)
Abstract Word Count: 176
Figure Count: 5
Supplemental Figure Count: 1
Supplemental Figure Table: 1

ABSTRACT

Motor neuron (MN) diseases are progressive disorders resulting from degeneration of neuromuscular junctions (NMJs), which form the connection between MNs and muscle fibers. NMJ-in-a-dish models have been developed to examine human MN-associated dysfunction with disease; however such co-culture models have randomly oriented myotubes with immature synapses that contract asynchronously. Mechanically patterned (MP) extracellular matrix with alternating soft and stiff stripes improve current NMJ-in-a-dish models by inducing both mouse and human myoblast durotaxis to stripes where they aligned, differentiated, and fused into patterned myotubes. Versus conventional culture on rigid substrates or unpatterned hydrogels, MP substrates supported increased differentiation, fusion, significantly larger acetylcholine receptor (AchR) clusters, and increased expression of MuSK and Lrp4, two cell surface receptors required for NMJ formation. Robust contractions were observed when mouse myotubes were stimulated by acetylcholine, with twitch duration and frequency most closely resembling mature muscle on MP substrates. Fused myotubes, when co-cultured with MNs were able to form even larger NMJs. Thus MP matrices produce more functionally active NMJs-in-a-dish, which could be used to elucidate disease pathology and to facilitate drug discovery.

INTRODUCTION

Neuromuscular junctions (NMJs) are specialized synapses that form between motor neurons (MNs) and skeletal muscle fibers. Upon activation, presynaptic MNs release acetylcholine (ACh) into the synaptic cleft, which then binds to acetylcholine receptors (AChRs) present on the postsynaptic muscle membrane; AChR ligation induces muscle

fiber contraction. Diseases affecting MNs, such as amyotrophic lateral sclerosis (ALS), are characterized by the loss of NMJs as MNs degenerate during disease progression (Wijesekera and Leigh, 2009; Viollet and Melki, 2013). This class of diseases is particularly debilitating as MN loss leads to muscle atrophy and paralysis and is often fatal. With limited treatment options that only extend lifespan by months (Engler *et al.*, 2004), significant efforts have focused on refining *in vivo* disease models to test new therapeutic options. However, current animal models for many MN diseases only replicate a portion of the spectrum of phenotypes in human disease (Pioro and Mitsumoto, 1995; Picher-Martel *et al.*, 2016).

Co-culture systems to create NMJs *in vitro* were developed to address concerns about animal models (Das *et al.*, 2007; Das *et al.*, 2010); more recent versions use stem cell-derived MNs and cell line- (Umbach *et al.*, 2012; Morimoto *et al.*, 2013; Uzel *et al.*, 2016), primary- (Chipman *et al.*, 2014; Steinbeck *et al.*, 2016), or stem cell-derived muscle (Demestre *et al.*, 2015; Puttonen *et al.*, 2015). Using human induced pluripotent stem cells in such systems has further enabled patient-specific MN disease modeling (Faravelli *et al.*, 2014; Abujarour and Valamehr, 2015; Lenzi *et al.*, 2016) and drug screening (Inoue *et al.*, 2014). Yet while having human cells enables more complex NMJ-in-a-dish modeling, concerns about MN, skeletal muscle, and NMJ maturity have been raised (Siller *et al.*, 2013). Moreover, NMJ development relies on the organization of embryonic muscle fibers, precise guidance of MN axons, and the interplay of signaling from both the pre- and postsynaptic cells (Witzemann, 2006; Wu *et al.*, 2010; Singhal and Martin, 2011; Shi *et al.*, 2012). Traditional unpatterned *in vitro* co-culture models on rigid substrates do not faithfully recapitulate the complex architecture observed *in vivo*; myotubes exhibit poor fusion efficiency and are highly disorganized, leading to inefficient and irregular contraction (Das *et al.*, 2007; Das *et al.*, 2010; Guo *et al.*, 2011; Umbach *et al.*, 2012). Unpatterned NMJ cultures also do not develop sufficiently large AChR clusters, postsynaptic membrane specializations that are a hallmark of functional, mature NMJs (Witzemann, 2006).

To improve cell and NMJ maturation in co-culture systems, some studies have employed microcontact printing (μCP), topography, and three-dimensional molds to organize myotubes *in vitro*. μCP guides cell growth by constraining cells to areas where extracellular matrix (ECM) proteins have been selectively deposited (Chen *et al.*, 1997). Myoblasts attach and fuse on patterned ECM, creating aligned myotubes (Engler *et al.*, 2004; Altomare *et al.*, 2010). Over time, however, proteins from culture media may deposit on the substrate, obscure the pattern, and eliminate cell alignment (Choi *et al.*, 2012b). Physical stimuli, including topographical cues, have also been employed to align myotubes *in vitro* (Wang *et al.*, 2012), but these systems employ substrates orders of magnitude more rigid than muscle (Choi *et al.*, 2012a). They often result in muscle that is thinner and less mature than their *in vivo* counterparts (Gaudel *et al.*, 2008; Zhu *et al.*, 2011; Lawlor *et al.*, 2014; Gibbons *et al.*, 2016). Both of these approaches rely on 2D methods, so 3D models have been developed that create aligned myobundles, which persist for several weeks in culture. Generally, these constructs are produced by using micromolds in which myoblasts are cultured (Morimoto *et al.*, 2013; Madden *et al.*, 2015; Bettadapur *et al.*, 2016) or via self assembly around T-shaped flexible posts (Sakar *et al.*, 2012; Cvetkovic *et al.*, 2014; Raman *et al.*, 2016); however, both are often fabricated with complicated lithography processes and resultant systems are difficult to process and image based on their 3D structure.

Methods that produce mature muscle but also rely on simple fabrication methods could be optimal for widespread use in NMJ-in-a-dish models. In this work, we describe a simple mechanically-patterned hydrogel that can be used as a MN and myotube co-culture platform. The system is based on a micropatterned hydrogel cell culture substrate that aligns cultured myotubes by juxtaposing soft and stiff regions similar to the alternating pattern of aligned myotubes with adjacent softer neurons to innervate the firm muscle *in vivo* (Choi *et al.*, 2012b). Such patterns result in improved fusion, differentiation, and AChR formation for cells of either mouse or human origin that are responsive to pharmacological stimuli and, upon co-culture with MNs, form functional NMJs, thus providing a significant improvement over standard cell culture vessels without the requirement of expensive specialized equipment.

RESULTS

Design and Fabrication of Mechanically Patterned Hydrogels

We developed a two-step photopolymerization method that produces PA hydrogels containing a grating pattern with alternating elasticity profiles (Fig. 1A), resulting in a hydrogel with 100 μm-wide “stiff” stripes interspersed with 200 μm-wide “soft” stripes, i.e. alternating regions of 12.6 ± 0.63 kPa and 0.72 ± 0.05 kPa, respectively as measured by atomic force microscopy (Fig. 1B). Using this method, we have successfully fabricated a wide range of geometrical patterns with micron-sized features. A sharp change in stiffness was observed at the interface of soft and stiff regions creating a steep gradient of > 100 kPa/mm consistent with prior observation (Vincent *et al.*, 2013) and indicating that there was limited diffusion during photopolymerization. For this NMJ-in-a-dish system, we chose to model myogenic and neurogenic stiffness (Engler *et al.*, 2006), though elastic properties can be easily modified by changing acrylamide concentrations and micropattern dimensions for alternate applications.

Improved Myotube Fusion and Differentiation on Mechanically Patterned Hydrogels

Mouse and hESC-derived myoblasts (Caron *et al.*, 2016) were cultured on mechanically patterned hydrogels to assess the influence of mechanical patterning on myotube fusion and differentiation. To decouple the effect of the compliant hydrogel from the mechanical patterning, myoblasts were also cultured on an unpatterned, myogenic hydrogel and on glass. Within 24 h, myoblasts preferentially migrated to and aligned with the stiffer myogenic regions on the mechanically patterned hydrogel while myoblasts on the unpatterned hydrogels and glass exhibit no organization (Fig. 2), consistent with myocytes and stem cells (Choi *et al.*, 2012b; Vincent *et al.*, 2013; Wen *et al.*, 2015). Prior to differentiation, myoblasts on patterned hydrogels also expressed more mRNA of M- and N-cadherin, markers indicative of cell fusion (Fig. 2).

After myogenic differentiation was initiated, elongated and multinucleated myotubes were present on all three substrates. However, the fusion index and average myotube width was larger on the mechanically patterned substrates compared to both the unpatterned myogenic hydrogel and glass (Fig. 3A-C); myotubes only on patterned hydrogels approach sizes consistent with *in vivo* muscle, independent of species (Gaudel *et al.*, 2008; Zhu *et al.*, 2011; Lawlor *et al.*, 2014; Gibbons *et al.*, 2016). In addition to fusion indices, mouse myoblasts expressed MyoD and myogenin transcription factors on mechanically patterned hydrogels in a temporally-regulated manner (Fig. 3D), consistent with their sequential expression during differentiation (Choi *et al.*, 2012a). Mechanically patterned human myotubes also expressed significantly more MHC transcript, while mouse myotubes trended toward higher expression,

suggesting that they are more mature than myotubes cultured on unpatterned myogenic hydrogels or glass (Fig. 3E, F). Together these data suggest that alignment, in addition to substrate elastic properties, could drive maturation and fusion, which may also contribute to deficiencies previously observed in hESC-derived myotube fusion (Demestre *et al.*, 2015; Puttonen *et al.*, 2015).

Mechanical Patterning Drives Formation of Functional Acetylcholine Receptor Clusters

AChRs are a critical component of NMJs and must be clustered in fused myotubes to function (Huh and Fuhrer, 2002). MNs secrete agrin to induce clustering, so upon addition of exogenous agrin, we determined if mechanical patterning could enhance AchR clustering. For both human and mouse, we found the largest AChR cluster sizes in myotubes cultured on mechanically patterned hydrogels (Fig. 4A-B). During NMJ development, agrin is released from approaching MNs and binds a receptor complex on the myotube consisting of dimers of muscle-specific receptor tyrosine kinase MuSK and low-density lipoprotein receptor-associated protein Lrp4, initiating a signaling cascade that induces AchR clustering (Fig. 4C) (Wu *et al.*, 2010; Shi *et al.*, 2012) .Lrp4 transcript was most expressed in myotubes in mechanically patterned myotubes, independent of species (Fig. 4D). MuSK transcript was similarly highest with mechanically patterned hydrogels, but only in human myotubes (Fig. 4E). To establish if endogenous agrin from MN co-culture could drive cluster formation, primary MNs were co-cultured after myoblast fusion into myotubes. Co-cultures were initiated after 4 d of myotube differentiation and maintained for 7 d. We found that mechanically patterned hydrogels drove formation of the largest AChR clusters, while AchR clusters on both the glass and unpatterned myogenic substrates remain small and punctate (Fig. 5A-B). In the co-culture system, MNs generally reside on top of the existing regions of mechanically patterned myotubes, avoiding the softer areas, and extend neurite outgrowths that terminate on the myotubes with some instances of co-localization with AchR clusters, an indicator of putative NMJ formation (Fig. 5C). Together these data suggest that NMJ-in-a-dish systems should support robust myotube alignment to facilitate AChR clustering, but these data do not yet establish the propagation of signals across the forming NMJ.

Spontaneous contractions were observed for myotube cultures only with mechanically patterned hydrogels (Fig. 6A,B left panels); spontaneous activity increases during development, thus our data is consistent with mechanically patterned myotubes being more functionally mature versus unpatterned myotubes (Altomare *et al.*, 2010). While these data suggest functional clusters in the NMJ-in-a-dish system, they do not establish if the junctions are indeed functional. To determine if AChR clusters could stimulate contraction, a bolus of 1 mM Acetylcholine was exogenously added. Upon stimulation, myotubes on both glass and mechanically patterned hydrogels contracted, though mechanically patterned myotubes underwent larger displacements during contraction, indicating a more intense contraction (Fig. 6A,B right panels). Mechanically patterned myotube contractions were also shorter in duration and occurred at a higher frequency than myotube contractions on glass (Fig. 6C,D), again suggesting that the AChR clusters, which are a critical component of NMJs, are more functionally mature.

Substrate Compliancy Mediates Clustering of Acetylcholine Receptors on Mechanically Patterned Hydrogels

To examine the roles of culture substrate stiffness versus myotube fusion and assembly in AchR clustering during NMJ development on mechanically patterned hydrogels, we cultured mouse myoblasts on patterned hydrogels with pathological stiff regions (Fig. 7).

After denervation, a hallmark of MN diseases, muscle fiber atrophy is accompanied by increased fibrosis, which increases the elastic modulus of muscle tissue (Engler *et al.*, 2004; Carlson, 2014). Thus, we fabricated mechanically patterned hydrogels with alternating soft (0.8 kPa) and pathological (58.1 kPa) stripes (Fig. 7A). Mouse myoblasts differentiated on the pathological patterns showed no difference in fusion or myotube width compared to those cultured on patterned substrates with myogenic stiff regions (Fig. 7B-C). AchR cluster area was sensitive to elastic modulus, with myotubes cultured on the pathological patterns expressing smaller AchR clusters than those cultured on myogenic mechanically patterned substrates (Fig. 7D-E), indicating that a previously unknown mechanotransduction pathway mediates AchR clustering. However, there was no correlation between myotube width and the size of the AchR clusters it expressed (Fig. 7F), indicating that the mechanism of AchR clustering is independent of the extent of myotube fusion.

DISCUSSION

Despite the proliferation of culture methods to assemble NMJs (Das *et al.*, 2007; Das *et al.*, 2010; Umbach *et al.*, 2012; Morimoto *et al.*, 2013; Chipman *et al.*, 2014; Faravelli *et al.*, 2014; Inoue *et al.*, 2014; Abujarour and Valamehr, 2015; Demestre *et al.*, 2015; Puttonen *et al.*, 2015; Lenzi *et al.*, 2016; Steinbeck *et al.*, 2016; Uzel *et al.*, 2016) and probe their mechanics,(Tay *et al.*, 2016) the possibility of functional neuron-to-muscle connectivity remains insufficiently validated due to technical limitations with *in vitro* co-culture systems. The mechanically patterned hydrogel system described here creates more mature (and wider) myotubes with larger AChR clusters that are more responsive to ACh and functional in co-culture versus conventional or topographically patterned substrates; this is likely the result of agrin secretion by MN, which signals through MuSK and Lrp4 to induce NMJ assembly (Wu *et al.*, 2010). Forced clustering of myotubes on stiffer stripes also likely drives alignment by overlapping their traction forces as well as increasing the probability that M- and N-cadherin-rich regions will make contact between cells, a step that is required for fusion (Choi *et al.*, 2012a; Choi *et al.*, 2012b). Alignment of hESC-derived myotubes also illustrates that mechanical patterns may help specify muscle during development and provides a platform for drug discovery.

During NMJ development, AchR clustering initiated by agrin signaling is a hallmark of the maturing NMJ synapse (Huh and Fuhrer, 2002; Witzemann, 2006). On the mechanically patterned culture system, AchR clustering significantly improves when compared to both the glass and unpatterned myogenic culture substrates (Fig. 4). Additionally, we found that under co-culture conditions, in which the myotubes are exposed to endogenous agrin released from MNs, mechanically patterned myotubes exhibit AchR clusters that are over 20x larger than those that occur in myotube monocultures treated with rat recombinant agrin; however, myotubes cultured on glass or unpatterned myogenic substrates do not respond in such a robust manner (Figs. 4B, 5B). We attribute the improved clustering to the fact that the MNs likely continuously release agrin onto the myotubes at a physiologically relevant level, while in the monoculture, myotubes were exposed to only one bolus dose of agrin added to the culture medium at day 1 after the onset of differentiation. Myotubes cultured on the mechanically patterned substrate, but not on glass or unpatterned myogenic substrates, express upregulated levels of Lrp4 transcript (Fig. 4D). Lrp4 acts as a receptor for agrin and through its interactions with MuSK, initiates an intracellular cascade that results in AchR clustering on the muscle surface (Kim *et al.*, 2008; Zhang *et al.*, 2008). Thus, lower expression levels of Lrp4 in myotubes grown on glass and unpatterned myogenic substrates may preclude their ability to respond to the improved agrin signaling that

occurs in the co-culture system.

To probe the role of substrate stiffness versus myotube alignment and fusion in the formation of AchR clusters, mouse myotubes were differentiated on patterned substrates of pathological stiffness. Cluster size was responsive to substrate stiffness, with smaller clusters expressed on pathological patterns, though there was no change in the extent of myotube fusion (Fig. 7). These data suggest that AchR cluster size is regulated independently of myotube fusion, i.e. clusters do not increase in size with increased myotube fusion, thus indicating a novel role for mechanotransduction in the control of AchR clustering. This pathway may be mediated by Wnt signaling, which has been shown to be responsive to mechanical cues, and is involved in the Lrp4/MuSK signal cascade leading to AchR clustering (Henriquez and Salinas, 2012; Du *et al.*, 2016). Mechanosensitivity of the NMJ may have implications for MN or muscle diseases in which muscle fibrosis occurs such as ALS and Duchenne muscular dystrophy, and may contribute insight into the mechanisms of muscle denervation and atrophy (Klingler *et al.*, 2012; Carlson, 2014).

While this system is relatively straightforward to assemble, several important caveats should be considered relative to existing systems. Most notably, we find that this system enables imaging for days in co-culture, which is sufficient for nascent NMJs to form; beyond that time, our system exhibits similar delamination issues to other 2D technologies (Wang *et al.*, 2012), which could limit long-term utility with disease modeling. 3D systems, despite complex fabrication, could provide long-term monitoring of patient-derived NMJs, though *in vitro* efforts in 3D to date have primarily focused on muscle (Sakar *et al.*, 2012; Cvetkovic *et al.*, 2014; Madden *et al.*, 2015; Bettadapur *et al.*, 2016; Raman *et al.*, 2016). A second consideration is the relative maturity of the junctions themselves; AChR clusters resemble more plaque-like morphology (Marques *et al.*, 2000; Huh and Fuhrer, 2002) and muscle twitch duration is long,(Schiaffino and Reggiani, 2011; Umbach *et al.*, 2012) even when improved by mechanical patterning, suggesting formation of functional but fetal-like synapses and immature slow fiber type muscles. While only spontaneous contractions induced by MNs were examined here, improved optogenetic control could further tease out NMJ maturity by examining signal propagation across junctions. Indeed optogenetic control of muscle in these types of systems has shown that human cells can be optically controlled to examine more complex behaviors in-a-dish (Sakar *et al.*, 2012; Raman *et al.*, 2016).

Despite these caveats, benefits specific to this NMJ-in-a-dish model are its relative ease of fabrication and the observation that mechanical patterning improves the maturation of hESC-derived skeletal muscle (Caron *et al.*, 2016). Other studies have illustrated that human progenitors can be used to create functional NMJs (Demestre *et al.*, 2015; Puttonen *et al.*, 2015), but to the best of our knowledge, this is the first demonstration that human myoblasts can be matured, fuse into patterned myotubes, and form functional NMJs *in vitro*. They appear to express more Lrp4 and MuSK and are more ACh sensitive versus these other efforts, so NMJs in these cells may represent a more mature state; however, side-by-side comparisons of these 2D methods is required to draw a better supported conclusion. In addition, this system reveals that a mechanotransductive pathway that is not dependent on myotube fusion influences the formation of AchR clusters and may mediate the cellular response to pathological conditions, such as fibrosis that occurs in muscle diseases. Thus we believe that this system represents the most straightforward and useful 2D NMJ-in-a-dish model for studying NMJ development and MN or muscle disease pathophysiology.

METHODS

Mechanically Patterned Gel Fabrication

Mechanically patterned hydrogels were fabricated using a two-step polyacrylamide (PA) photopolymerization method (Fig. 1A), modified from established methods (Marklein and Burdick, 2010; Tse and Engler, 2010) but which differs from prior sequential polymerization methods (Choi *et al.*, 2012b). First, single-modulus PA hydrogels were polymerized onto methacrylated 18-mm glass coverslips from a prepolymer solution containing acrylamide (3%), bis-acrylamide (0.4%) and 2-hydroxy-4'-(2-hydroxyethoxy)-2-methylpropiophenone (0.5%). The prepolymer solution was sandwiched between the methacrylated glass and a chloro-silanated glass slide and exposed to ultraviolet light (350 nm) for 5 min. Following polymerization, the PA hydrogel was removed from the chloro-silanated glass slide, dehydrated overnight, then rehydrated with a second prepolymer solution consisting of acrylamide (4% for myogenic mechanically patterned substrates and 4.5% for pathological mechanically patterned substrates), bis-acrylamide (0.4%) and 2-hydroxy-4'-(2-hydroxyethoxy)-2-methylpropiophenone (0.5%). The rehydrated PA gel was exposed to ultraviolet light (350 nm) for 5 min through a high-resolution chrome photomask patterned with alternating black (200 μm width) and clear (100 μm width) stripes. The resultant pattern on the PA hydrogel was softer 200 μm wide stripes alternating with stiffer 100 μm wide stripes. The bis-acrylamide concentration was maintained at a relatively high 0.4% w/v concentration to minimize the amount of differential swelling that may occur in adjacent stripes (Charest *et al.*, 2012; Choi *et al.*, 2012a).

To fabricate single modulus myogenic PA hydrogels, a prepolymer solution consisting of acrylamide (6.25%), bis-acrylamide (0.4%) and 2-hydroxy-4'-(2-hydroxyethoxy)-2-methylpropiophenone (0.5%) was used. Following polymerization, the hydrogels were washed thoroughly with phosphate buffered saline (PBS) to remove any unreacted monomer or crosslinker and stored in PBS at 4°C.

The surfaces of the mechanically and myogenic hydrogels were functionalized with collagen IV using a photoactivating crosslinker, Sulfo-SANPAH (Pierce). The hydrogels were immersed in HEPES buffer (pH 8.4, 50 mM) containing sulfo-SANPAH (0.2 mg/mL) and exposed to ultraviolet light (350 nm) for 10 min. After several washes in PBS, the hydrogels were incubated in collagen IV (100 μg/mL) overnight at 37°C.

Mechanical Characterization

Substrate stiffness was measured via indentation using an MFP-3D-Bio (Asylum Research, Santa Barbara, CA) atomic force microscope (AFM). Chromium/gold-coated, silicone nitride (SiN) cantilevers with pyramid tips (PNP-TR; NanoWorld) with a nominal spring constant of ~30 pN/nm as determined from the MFP-3Ds built-in thermal calibration function were used. Samples were mounted on glass slides using vacuum grease and immersed in PBS. The probe was indented into the sample with an approach velocity 2 μm/s and a force trigger of 2 nN. AFM data was analyzed using custom code in Igor Pro (Wavemetrics); the substrate spring constant, i.e., Young's Moduli, was determined using a linearized Sneddon model (Kaushik *et al.*, 2011).

Cell Line and Human embryonic stem cell (hESC)-derived Myotube Culture

C2C12 mouse myoblast cell line, which was validated by ATCC (CRL-1772), was seeded on the surface of mechanically patterned and myogenic hydrogels or glass coverslips coated with collagen IV (100 μg/mL) at a density of 4000 cells cm^{-2} and

maintained in growth medium consisting of Dulbecco's modified Eagle's medium (DMEM, with 4.5 g/L glucose, with glutamine, without sodium pyruvate), fetal bovine serum (20%) and penicillin/streptomycin (1%). After 2 d in growth medium, the cultures were switched to differentiation medium consisting of DMEM, horse serum (2%), insulin (2 µg/mL) and penicillin/streptomycin (1%). At 1 d after the onset of differentiation cultures were treated with agrin (100 ng/mL) to induce AChR clustering and at 2 d after the onset of differentiation cultures were treated with cytosine β-D-arabinofuranoside (10 µM) to inhibit myoblast proliferation. At 5 d after the onset of differentiation, cultures were either assayed for functional activity or terminated for immunofluorescence and RNA analysis.

Human embryonic stem cell (hESC)-derived myoblasts (GENEA002) were obtained and validated by Genea Biocells (La Jolla, CA) through prior publication (Caron *et al.*, 2016). Cells were seeded onto hydrogels or glass coverslips coated with collagen I (100 µg/mL) at a density of 15k cells/cm^2 and maintained in growth medium (SKM-02; Genea Biocells) for 3 d. Cultures were then changed to differentiation medium (SKM-03; Genea Biocells) and maintained for 7 d prior to functional analysis or fixation for immunofluorescence and RNA analysis.

Isolation of Rat Primary MNs and their Co-Culture with Myotubes

The use of rats in this study was approved by UC San Diego's IACUC review board (protocol # S11032). Mouse embryonic motor neurons were isolated from the spinal cords embryonic day 12 CD1 mouse embryos using a discontinuous density gradient centrifugation purification technique.(Gingras *et al.*, 2007) Purified motor neurons were co-cultured with established C2C12 myotube cultures at 4 d after the onset of myotube differentiation. The co-cultures were maintained in motor neuron medium consisting of Neurobasal medium, B27 supplement (2%), glutamine (0.5 mM), hydrocortisone (400 ng/mL), insulin (2 µg/mL), fetal bovine serum (10%), and penicillin/streptomycin (1%).

Immunofluorescence Staining, Fusion Characterization and AChR Characterization

Cultures were fixed with 3.7% formaldehyde for 25 min at room temperature, permeabilized with 1% Triton-X for 5 min, then incubated in PBS containing 5% goat serum for 20 min at room temperature. Samples were incubated in primary antibodies at 4°C overnight, washed in PBS, then incubated in secondary antibodies for 45 min at room temperature, followed by a 10 min incubation in Hoechst 33352 (1:1000 in PBS) to counterstain nuclei. Primary antibodies used in this study were hybridoma-derived anti-myosin heavy chain (1:50, MF20, DSHB) and rabbit polyclonal anti-β-III-Tubulin (1:500, Abcam ab18207). Alexa Fluor 488 secondary antibody was used (1:1000, Fisher Scientific). To label AChR clusters, samples were incubated with α-bungarotoxin (BTX) conjugated with Alexa Fluor 555 (1:500, Molecular Probes) for 45 min at room temperature.

Myoblast fusion index was calculated as the percentage of Hoechst-positive cell nuclei residing within MF20-positive myotubes. Average myotube width was calculated by measuring the width at the widest point on the myotube using the ImageJ measure function. For each metric, data was collected from 20 representative 20x images. BTX-immunoreactivity on 5 (mouse) or 20 (human) representative 60x images was used to evaluate AChR clustering. Average cluster size was quantified by manual tracing using ImageJ software. The width of each myotube that expressed AchR clusters was

recorded and plotted against AchR cluster area to evaluate the correlation between cluster size and myotube width.

Quantitative Polymerase Chain Reaction
RNA was collected from cultures using Trizol isolation and cDNA was synthesized from 2 μg of RNA using reverse transcriptase polymerase chain reaction (37°C for 60 min, 99°C for 5 min and 5°C for 5 min) with Superscript II Reverse transcriptase (Invitrogen) and 2.5 mM random hexamer mix (Invitrogen). Quantitative polymerase chain reaction was carried out using a CFX96 Real-Time PCR Detection system using iQ SYBR Green Supermix (2 min at 50°C followed by 10 min at 95°C for one cycle, then 15s at 95°C followed by 1 min at 60°C for 40 cycles) and custom designed primers (Table S1). Expression levels were calculated based on a standard curve generated by fibronectin plasmid. All data was normalized to GAPDH and data from the myogenic and MP hydrogels was presented as the fold change from the glass control.

Functional Assessment of Myotubes
Brightfield video-images were acquired with a CoolSnap HQ camera (Photometrics Scientific) through a Nikon Eclipse Ti inverted microscope with a 10x objective. Myotube monocultures were assessed for ACh responsiveness after 5 d in culture (mouse) or 7 d in culture (human). Videos were collected at 9.2 frames per second and were captured prior to and immediately after stimulation with 1 mM acetylcholine chloride (Sigma) in a 10 μL volume. Functional connectivity of hESC-MN-ChR2-YFP and myotubes were assessed at 3 d (mouse) or 7 d (human) after co-culture. Cells were stimulated with a Nikon Intensilight Illuminator through a 488 nm fluorescence filter and brightfield video-images were collected simultaneously. Kymographs of myotube contraction were generated using Image J software.

Statistical Analysis
All data were presented as the mean ± standard error of the mean. Statistical analysis was carried out with Graphpad Prism software using one-way analysis of variance (ANOVA) tests, unpaired t-test or linear regression analysis, as appropriate. Statistical significance was considered at $p < 0.05$.

ACKNOWLEDGEMENTS
The authors would like to thank Drs. Heather Main and Jamshid Arjomand (Genea Biocells) for use of hESC-derived myoblasts. The authors would also like to acknowledge funding support from the National Institutes of Health (DP2OD006460 to A.J.E. and F32HL131424 to C.L.H.) and National Science Foundation (1463689 to A.J.E.) as well as a support via the National Science Foundation Graduate Research Fellowship program (to A.K.G.).

REFERENCES
Abujarour, R., and Valamehr, B. (2015). Generation of skeletal muscle cells from pluripotent stem cells: advances and challenges. Front Cell Dev Biol *3*, 29.
Altomare, L., Riehle, M., Gadegaard, N., Tanzi, M.C., and Fare, S. (2010). Microcontact printing of fibronectin on a biodegradable polymeric surface for skeletal muscle cell orientation. Int J Artif Organs *33*, 535-543.
Bettadapur, A., Suh, G.C., Geisse, N.A., Wang, E.R., Hua, C., Huber, H.A., Viscio, A.A., Kim, J.Y., Strickland, J.B., and McCain, M.L. (2016). Prolonged Culture of Aligned Skeletal Myotubes on Micromolded Gelatin Hydrogels. Sci Rep *6*, 28855.

Carlson, B.M. (2014). The Biology of Long-Term Denervated Skeletal Muscle. Eur J Transl Myol *24*, 3293.
Caron, L., Kher, D., Lee, K.L., McKernan, R., Dumevska, B., Hidalgo, A., Li, J., Yang, H., Main, H., Ferri, G., Petek, L.M., Poellinger, L., Miller, D.G., Gabellini, D., and Schmidt, U. (2016). A Human Pluripotent Stem Cell Model of Facioscapulohumeral Muscular Dystrophy-Affected Skeletal Muscles. Stem Cells Transl Med.
Charest, J.M., Califano, J.P., Carey, S.P., and Reinhart-King, C.A. (2012). Fabrication of substrates with defined mechanical properties and topographical features for the study of cell migration. Macromol Biosci *12*, 12-20.
Chen, C.S., Mrksich, M., Huang, S., Whitesides, G.M., and Ingber, D.E. (1997). Geometric control of cell life and death. Science *276*, 1425-1428.
Chipman, P.H., Zhang, Y., and Rafuse, V.F. (2014). A stem-cell based bioassay to critically assess the pathology of dysfunctional neuromuscular junctions. PLoS One *9*, e91643.
Choi, Y.S., Vincent, L.G., Lee, A.R., Dobke, M.K., and Engler, A.J. (2012a). Mechanical derivation of functional myotubes from adipose-derived stem cells. Biomaterials *33*, 2482-2491.
Choi, Y.S., Vincent, L.G., Lee, A.R., Kretchmer, K.C., Chirasatitsin, S., Dobke, M.K., and Engler, A.J. (2012b). The alignment and fusion assembly of adipose-derived stem cells on mechanically patterned matrices. Biomaterials.
Cvetkovic, C., Raman, R., Chan, V., Williams, B.J., Tolish, M., Bajaj, P., Sakar, M.S., Asada, H.H., Saif, M.T., and Bashir, R. (2014). Three-dimensionally printed biological machines powered by skeletal muscle. Proc Natl Acad Sci U S A *111*, 10125-10130.
Das, M., Rumsey, J.W., Bhargava, N., Stancescu, M., and Hickman, J.J. (2010). A defined long-term in vitro tissue engineered model of neuromuscular junctions. Biomaterials *31*, 4880-4888.
Das, M., Rumsey, J.W., Gregory, C.A., Bhargava, N., Kang, J.F., Molnar, P., Riedel, L., Guo, X., and Hickman, J.J. (2007). Embryonic motoneuron-skeletal muscle co-culture in a defined system. Neuroscience *146*, 481-488.
Demestre, M., Orth, M., Fohr, K.J., Achberger, K., Ludolph, A.C., Liebau, S., and Boeckers, T.M. (2015). Formation and characterisation of neuromuscular junctions between hiPSC derived motoneurons and myotubes. Stem Cell Res *15*, 328-336.
Du, J., Zu, Y., Li, J., Du, S., Xu, Y., Zhang, L., Jiang, L., Wang, Z., Chien, S., and Yang, C. (2016). Extracellular matrix stiffness dictates Wnt expression through integrin pathway. Scientific reports *6*, 20395.
Engler, A.J., Griffin, M.A., Sen, S., Bonnemann, C.G., Sweeney, H.L., and Discher, D.E. (2004). Myotubes differentiate optimally on substrates with tissue-like stiffness: pathological implications for soft or stiff microenvironments. J Cell Biol *166*, 877-887.
Engler, A.J., Sen, S., Sweeney, H.L., and Discher, D.E. (2006). Matrix elasticity directs stem cell lineage specification. Cell *126*, 677-689.
Faravelli, I., Frattini, E., Ramirez, A., Stuppia, G., Nizzardo, M., and Corti, S. (2014). iPSC-Based Models to Unravel Key Pathogenetic Processes Underlying Motor Neuron Disease Development. J Clin Med *3*, 1124-1145.
Gaudel, C., Schwartz, C., Giordano, C., Abumrad, N.A., and Grimaldi, P.A. (2008). Pharmacological activation of PPARbeta promotes rapid and calcineurin-dependent fiber remodeling and angiogenesis in mouse skeletal muscle. Am J Physiol Endocrinol Metab *295*, E297-304.
Gibbons, M.C., Sato, E.J., Bachasson, D., Cheng, T., Azimi, H., Schenk, S., Engler, A.J., Singh, A., and Ward, S.R. (2016). Muscle architectural changes after Massive human rotator cuff tear. J Orthop Res.

Gingras, M., Gagnon, V., Minotti, S., Durham, H.D., and Berthod, F. (2007). Optimized protocols for isolation of primary motor neurons, astrocytes and microglia from embryonic mouse spinal cord. J Neurosci Methods *163*, 111-118.
Guo, X., Gonzalez, M., Stancescu, M., Vandenburgh, H.H., and Hickman, J.J. (2011). Neuromuscular junction formation between human stem cell-derived motoneurons and human skeletal muscle in a defined system. Biomaterials *32*, 9602-9611.
Henriquez, J.P., and Salinas, P.C. (2012). Dual roles for Wnt signalling during the formation of the vertebrate neuromuscular junction. Acta Physiol (Oxf) *204*, 128-136.
Huh, K.H., and Fuhrer, C. (2002). Clustering of nicotinic acetylcholine receptors: from the neuromuscular junction to interneuronal synapses. Mol Neurobiol *25*, 79-112.
Inoue, H., Nagata, N., Kurokawa, H., and Yamanaka, S. (2014). iPS cells: a game changer for future medicine. EMBO J *33*, 409-417.
Kaushik, G., Fuhrmann, A., Cammarato, A., and Engler, A.J. (2011). In situ mechanical analysis of myofibrillar perturbation and aging on soft, bilayered Drosophila myocardium. In: Biophys J, vol. 101, United States: 2011 Biophysical Society. Published by Elsevier Inc, 2629-2637.
Kim, N., Stiegler, A.L., Cameron, T.O., Hallock, P.T., Gomez, A.M., Huang, J.H., Hubbard, S.R., Dustin, M.L., and Burden, S.J. (2008). Lrp4 is a receptor for Agrin and forms a complex with MuSK. Cell *135*, 334-342.
Klingler, W., Jurkat-Rott, K., Lehmann-Horn, F., and Schleip, R. (2012). The role of fibrosis in Duchenne muscular dystrophy. Acta Myol *31*, 184-195.
Lawlor, M.W., Viola, M.G., Meng, H., Edelstein, R.V., Liu, F., Yan, K., Luna, E.J., Lerch-Gaggl, A., Hoffmann, R.G., Pierson, C.R., Buj-Bello, A., Lachey, J.L., Pearsall, S., Yang, L., Hillard, C.J., and Beggs, A.H. (2014). Differential muscle hypertrophy is associated with satellite cell numbers and Akt pathway activation following activin type IIB receptor inhibition in Mtm1 p.R69C mice. Am J Pathol *184*, 1831-1842.
Lenzi, J., Pagani, F., De Santis, R., Limatola, C., Bozzoni, I., Di Angelantonio, S., and Rosa, A. (2016). Differentiation of control and ALS mutant human iPSCs into functional skeletal muscle cells, a tool for the study of neuromuscolar diseases. Stem Cell Res *17*, 140-147.
Madden, L., Juhas, M., Kraus, W.E., Truskey, G.A., and Bursac, N. (2015). Bioengineered human myobundles mimic clinical responses of skeletal muscle to drugs. Elife *4*, e04885.
Marklein, R.A., and Burdick, J.A. (2010). Spatially controlled hydrogel mechanics to modulate stem cell interactions. Soft Matter *6*, 136-143.
Marques, M.J., Conchello, J.A., and Lichtman, J.W. (2000). From plaque to pretzel: fold formation and acetylcholine receptor loss at the developing neuromuscular junction. J Neurosci *20*, 3663-3675.
Morimoto, Y., Kato-Negishi, M., Onoe, H., and Takeuchi, S. (2013). Three-dimensional neuron-muscle constructs with neuromuscular junctions. Biomaterials *34*, 9413-9419.
Picher-Martel, V., Valdmanis, P.N., Gould, P.V., Julien, J.P., and Dupre, N. (2016). From animal models to human disease: a genetic approach for personalized medicine in ALS. Acta Neuropathol Commun *4*, 70.
Pioro, E.P., and Mitsumoto, H. (1995). Animal models of ALS. Clin Neurosci *3*, 375-385.
Puttonen, K.A., Ruponen, M., Naumenko, N., Hovatta, O.H., Tavi, P., and Koistinaho, J. (2015). Generation of Functional Neuromuscular Junctions from Human Pluripotent Stem Cell Lines. Front Cell Neurosci *9*, 473.
Raman, R., Cvetkovic, C., Uzel, S.G., Platt, R.J., Sengupta, P., Kamm, R.D., and Bashir, R. (2016). Optogenetic skeletal muscle-powered adaptive biological machines. Proc Natl Acad Sci U S A *113*, 3497-3502.

Sakar, M.S., Neal, D., Boudou, T., Borochin, M.A., Li, Y., Weiss, R., Kamm, R.D., Chen, C.S., and Asada, H.H. (2012). Formation and optogenetic control of engineered 3D skeletal muscle bioactuators. Lab Chip *12*, 4976-4985.
Schiaffino, S., and Reggiani, C. (2011). Fiber types in mammalian skeletal muscles. Physiol Rev *91*, 1447-1531.
Shi, L., Fu, A.K., and Ip, N.Y. (2012). Molecular mechanisms underlying maturation and maintenance of the vertebrate neuromuscular junction. Trends Neurosci *35*, 441-453.
Siller, R., Greenhough, S., Park, I.H., and Sullivan, G.J. (2013). Modelling human disease with pluripotent stem cells. Curr Gene Ther *13*, 99-110.
Singhal, N., and Martin, P.T. (2011). Role of extracellular matrix proteins and their receptors in the development of the vertebrate neuromuscular junction. Dev Neurobiol *71*, 982-1005.
Steinbeck, J.A., Jaiswal, M.K., Calder, E.L., Kishinevsky, S., Weishaupt, A., Toyka, K.V., Goldstein, P.A., and Studer, L. (2016). Functional Connectivity under Optogenetic Control Allows Modeling of Human Neuromuscular Disease. Cell Stem Cell *18*, 134-143.
Tay, A., Schweizer, F.E., and Di Carlo, D. (2016). Micro- and nano-technologies to probe the mechano-biology of the brain. Lab Chip *16*, 1962-1977.
Tse, J.R., and Engler, A.J. (2010). Preparation of hydrogel substrates with tunable mechanical properties. Curr Protoc Cell Biol *Chapter 10*, Unit 10 16.
Umbach, J.A., Adams, K.L., Gundersen, C.B., and Novitch, B.G. (2012). Functional neuromuscular junctions formed by embryonic stem cell-derived motor neurons. PLoS One *7*, e36049.
Uzel, S.G., Platt, R.J., Subramanian, V., Pearl, T.M., Rowlands, C.J., Chan, V., Boyer, L.A., So, P.T., and Kamm, R.D. (2016). Microfluidic device for the formation of optically excitable, three-dimensional, compartmentalized motor units. Sci Adv *2*, e1501429.
Vincent, L.G., Choi, Y.S., Alonso-Latorre, B., del Alamo, J.C., and Engler, A.J. (2013). Mesenchymal stem cell durotaxis depends on substrate stiffness gradient strength. Biotechnol J *8*, 472-484.
Viollet, L., and Melki, J. (2013). Spinal muscular atrophies. Handb Clin Neurol *113*, 1395-1411.
Wang, P.Y., Thissen, H., and Tsai, W.B. (2012). The roles of RGD and grooved topography in the adhesion, morphology, and differentiation of C2C12 skeletal myoblasts. Biotechnol Bioeng *109*, 2104-2115.
Wen, J.H., Choi, O., Taylor-Weiner, H., Fuhrmann, A., Karpiak, J.V., Almutairi, A., and Engler, A.J. (2015). Haptotaxis is Cell Type Specific and Limited by Substrate Adhesiveness. Cellular and Molecular Bioengineering *8*, 530-542.
Wijesekera, L.C., and Leigh, P.N. (2009). Amyotrophic lateral sclerosis. Orphanet J Rare Dis *4*, 3.
Witzemann, V. (2006). Development of the neuromuscular junction. Cell Tissue Res *326*, 263-271.
Wu, H., Xiong, W.C., and Mei, L. (2010). To build a synapse: signaling pathways in neuromuscular junction assembly. Development *137*, 1017-1033.
Zhang, B., Luo, S., Wang, Q., Suzuki, T., Xiong, W.C., and Mei, L. (2008). LRP4 serves as a coreceptor of agrin. Neuron *60*, 285-297.
Zhu, J., Li, Y., Lu, A., Gharaibeh, B., Ma, J., Kobayashi, T., Quintero, A.J., and Huard, J. (2011). Follistatin improves skeletal muscle healing after injury and disease through an interaction with muscle regeneration, angiogenesis, and fibrosis. Am J Pathol *179*, 915-930.

Figure Captions

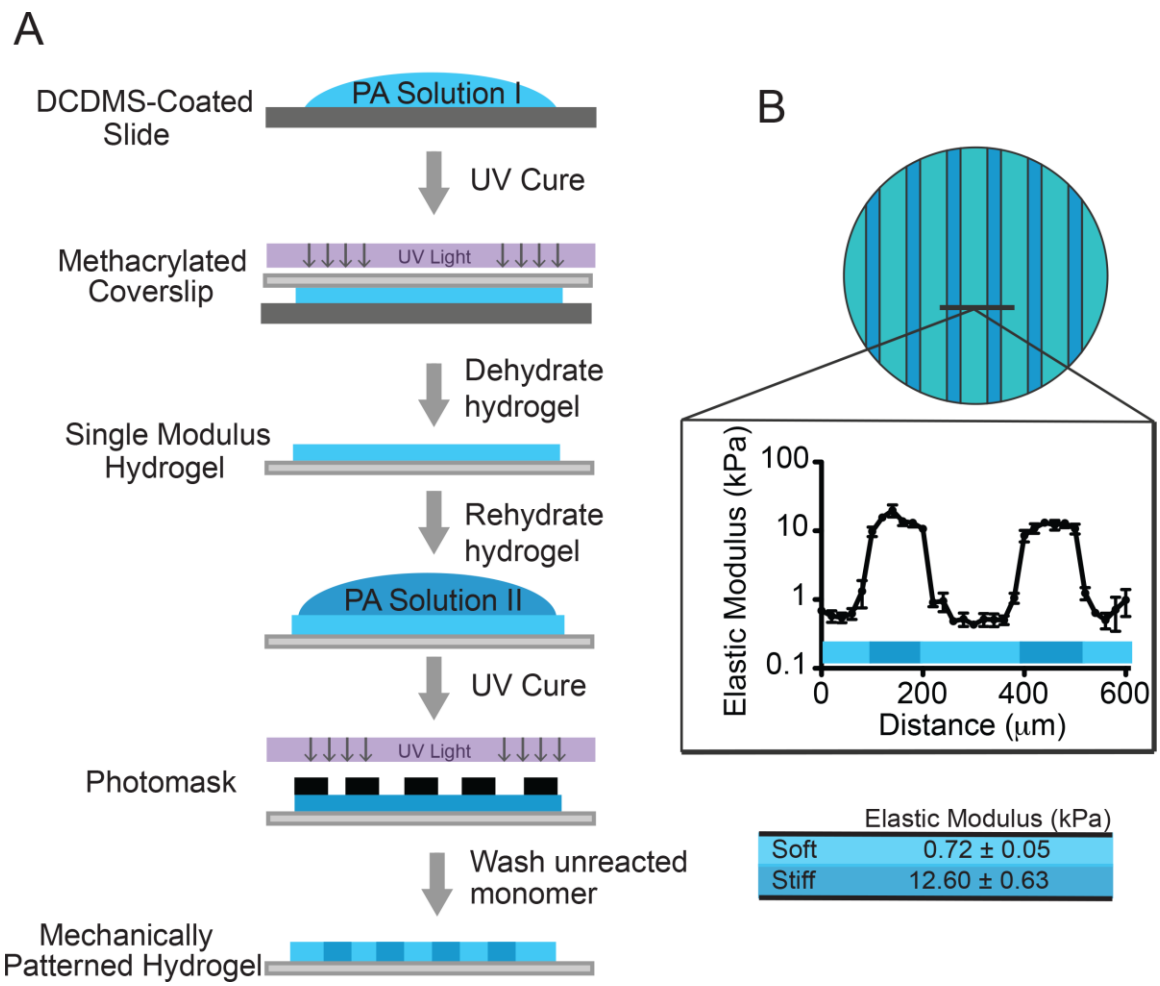

Fig. 1. Fabrication of Mechanically Patterned Hydrogel. (A) Schematic of patterning process where sequential exposures of the hydrogel to UV light, the second exposure including a photomask, created the patterned hydrogel. (B) Hydrogel pattern schematic and plot of elastic modulus versus position orthogonal to the pattern direction. Average modulus values for “soft” (teal) and “stiff” (blue) regions are shown.

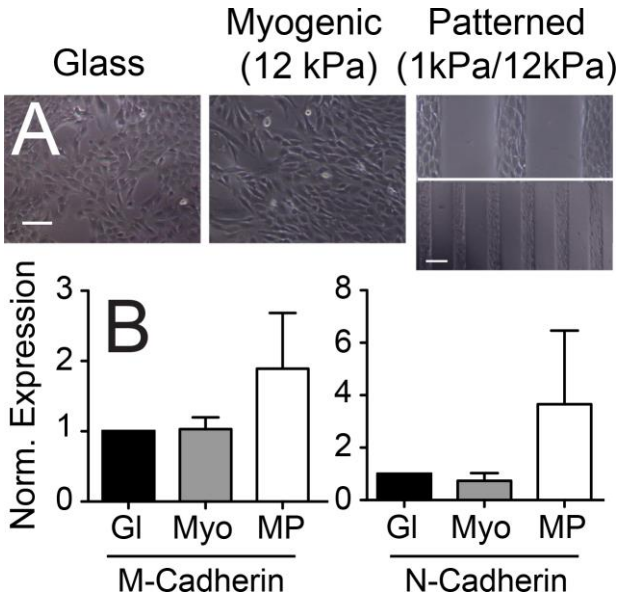

Fig. 2. Durotactic Pattern Recognition and Fusion Marker Expression. (A) Brightfield images of mouse myoblasts on the indicated substrates. Scale bar indicates 100 microns. Inset shows low magnification brightfield image of mouse myoblasts on the mechanically patterned substrate. Scale bar indicates 200 microns. (B) mRNA transcript levels for M-cadherin (left) and N-cadherin (right) for the indicated conditions. Data were normalized to glass substrates (n = 5).

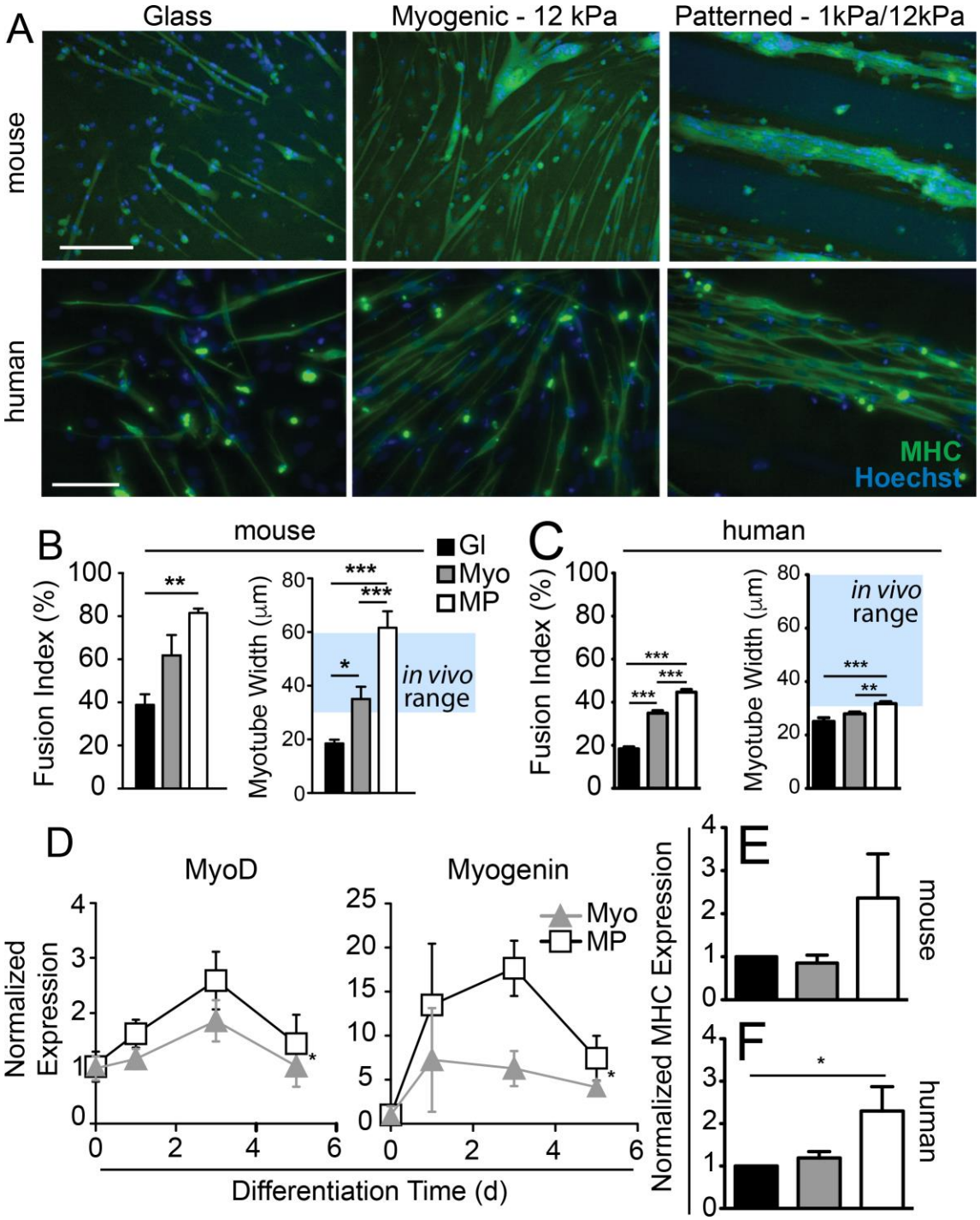

Fig. 3. Improved Myoblast Fusion and Differentiation on Mechanically Patterned Matrices. (A) Representative fluorescent images of myotubes cultured on glass, myogenic (MYO) or mechanically patterned (MP) hydrogels at 5 days (mouse) or 7 days (human) after induction of differentiation. Cells were immunolabeled for myosin heavy chain (green) and counterstained for nuclei with Hoeschst 33352 (blue). Scale bars indicate 30 μm. Fusion index (n = 10) and average myotube width (n = 30 – 88 individual myotubes per condition) are plotted for both (B) mouse and (C) human myotubes. Glass, myogenic substrates, and mechanically patterned hydrogels are plotted in green, blue, and purple, respectively. The shaded region denotes the *in vivo*

range of myotube width (Gaudel *et al.*, 2008; Zhu *et al.*, 2011; Lawlor *et al.*, 2014; Gibbons *et al.*, 2016). (D) mRNA expression of MyoD and Myogenin normalized to day zero for each condition plotted for the indicated number of days post induction of differentiation (n = 6). Data is shown for both substrates of myogenic stiffness, i.e. 12 kPa (blue), and with a mechanical pattern (purple) and expression levels are time-dependent ($p < 0.05$). (E) Myosin heavy chain (MHC) was assessed by qPCR, data normalized to GAPDH, and plotted for glass, myogenic substrates, and mechanically patterned hydrogels (n = 5). *$p<0.05$, **$p<0.01$, and ***$p<0.001$ based on ANOVA comparisons of the indicated groups.

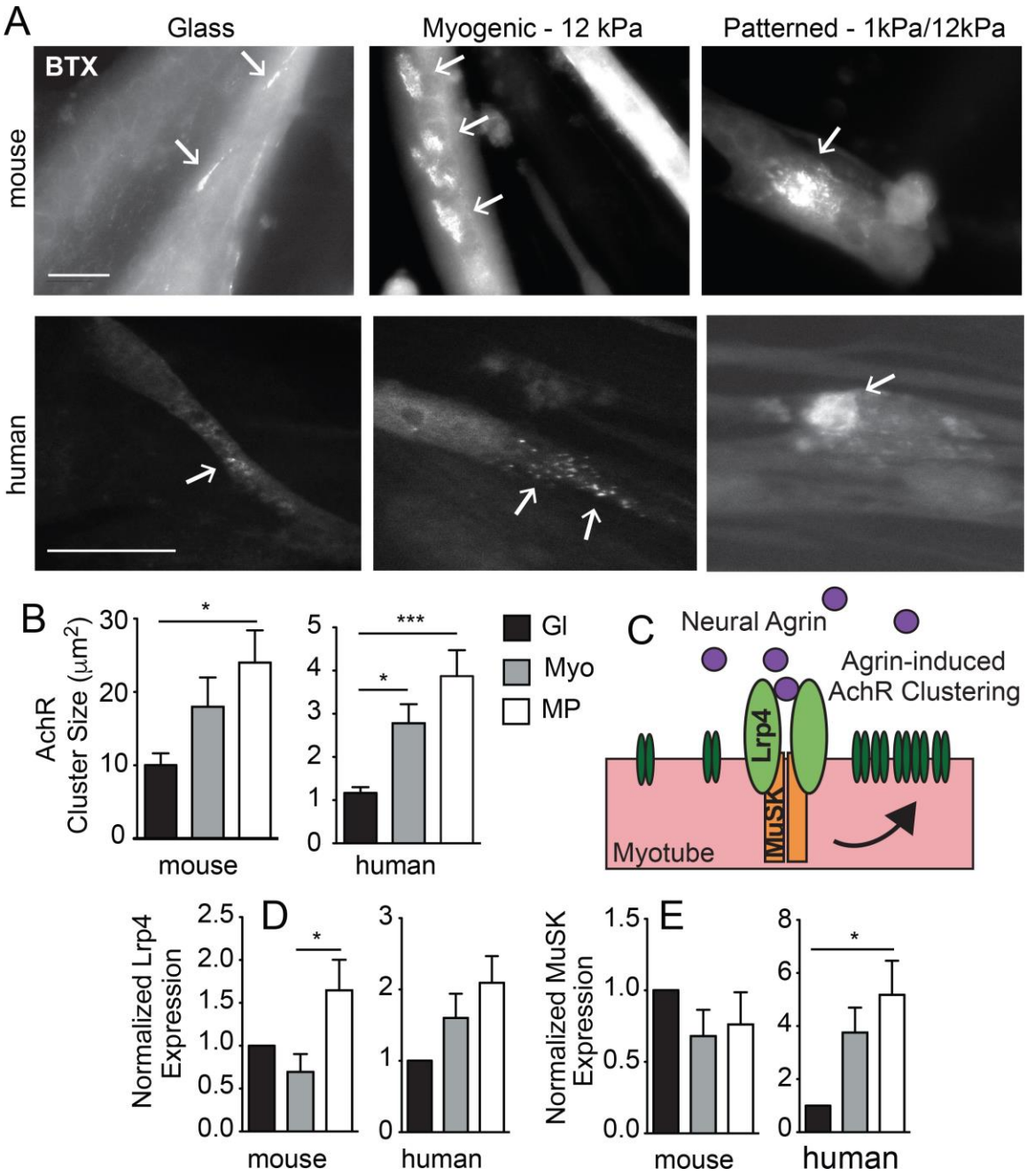

Fig. 4. Patterning Drives Clustering of Acetylcholine Receptors. (A) Representative fluorescent images of AchR clustering on agrin-treated myotubes cultured on glass, myogenic (MYO) or mechanically patterned (MP) hydrogels at 5 days (mouse) or 7 days (human) after induction of differentiation. AchRs were labeled with α-bungarotoxin (BTX). Scale bars indicate 25 μm. (B) Plot of average AchR cluster size for mouse (left, n =5) and human (right, n = 20). (C) Schematic of agrin-driven AchR clustering involving Lrp4 and MuSK. (D) Lrp4 and (E) MuSK expression was assessed by qPCR, data normalized to transcript expression on glass, and plotted for the indicated species (n = 6). Glass, myogenic substrates, and mechanically patterned hydrogels are plotted in green, blue, and purple, respectively. *p<0.05, **p<0.01, and ***p<0.001 based on ANOVA comparisons of the indicated groups.

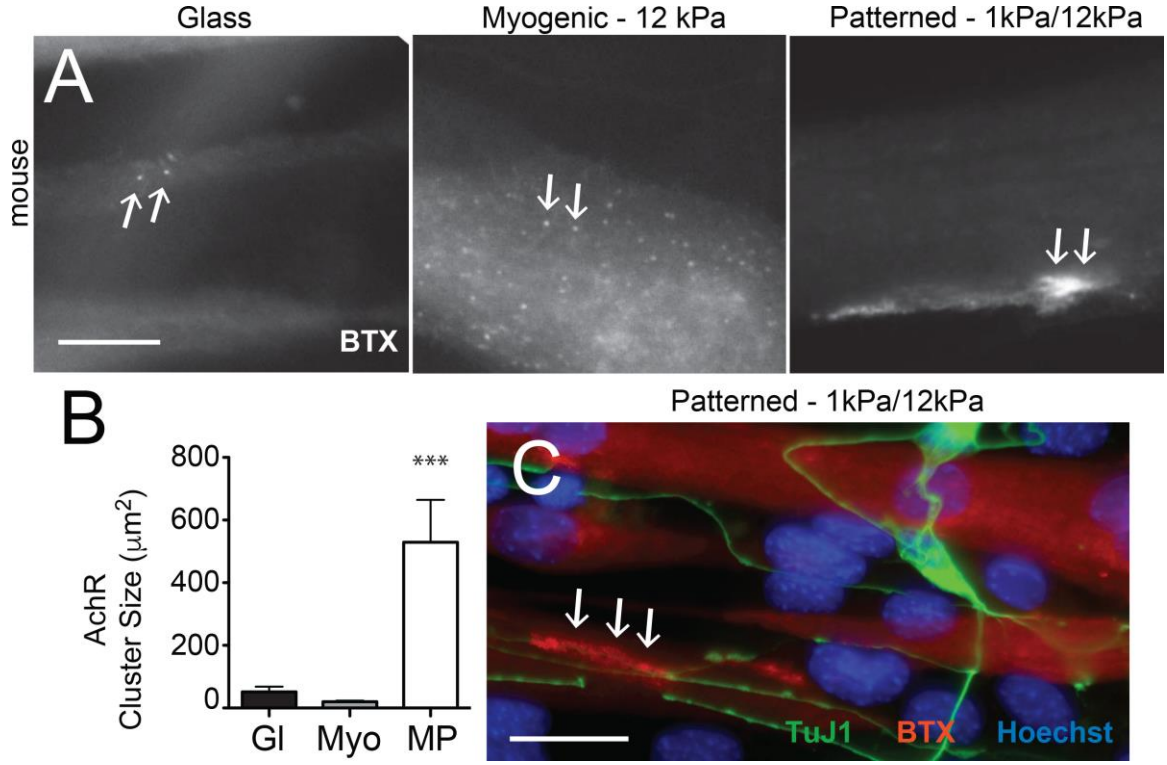

Fig. 5. Patterning Improves AChR Clusters Induced by MN Co-culture. (A) Representative fluorescent images of AchR clustering on mouse myotubes co-cultured with mouse MN for 7 d. Myotubes were differentiated for 4 d prior to the start of the co-culture. AchRs were labeled with α-bungarotoxin (BTX). Scale bar indicates 20 μm. Arrows indicate BTX immunoreactivity. (B) Plot of average AchR cluster size (n = 20) for glass (Gl), soft myogenic substrates (Myo) and mechanically patterned hydrogels (MP). ***p<0.001 based on ANOVA comparisons between substrate conditions. (C) Representative fluorescent image of patterned mouse myotube/mouse MN co-culture at 7 d. Cells were immunostained with β-III-tubulin (TuJ1, green), BTX (red) and counterstained for nuclei with Hoeschst 33352. Scale bar indicates 30 microns. Arrows indicate BTX immunoreactivity that colocalizes with β-III-tubulin immunoreactivity, suggestive of a putative NMJ.

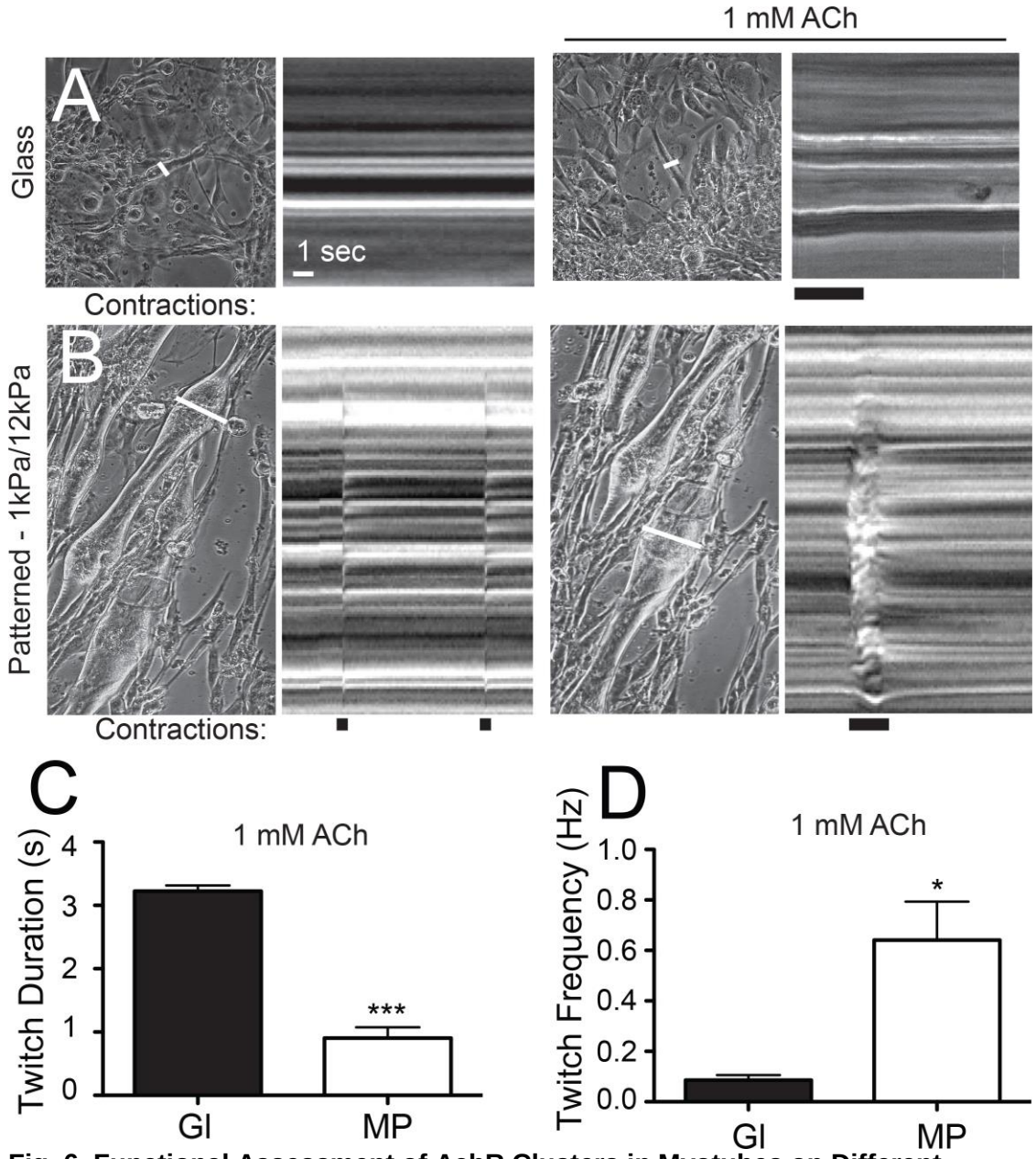

Fig. 6. Functional Assessment of AchR Clusters in Myotubes on Different Substrates. (A, B) Still movie images of myotube cultures are shown (left). The white line indicates which contracting myotube was used to create the associated kymograph (right). The black bar at the bottom of each kymograph notes contractions. Cultures were stimulated with Acetylcholine (Ach) as indicated. Plot of (C) twitch duration and (D) frequency for glass (GI; black) and mechanically patterned hydrogels (MP; white) (n = 5). *p<0.05, **p<0.01, and ***p<0.001 based on ANOVA comparisons between substrate conditions.

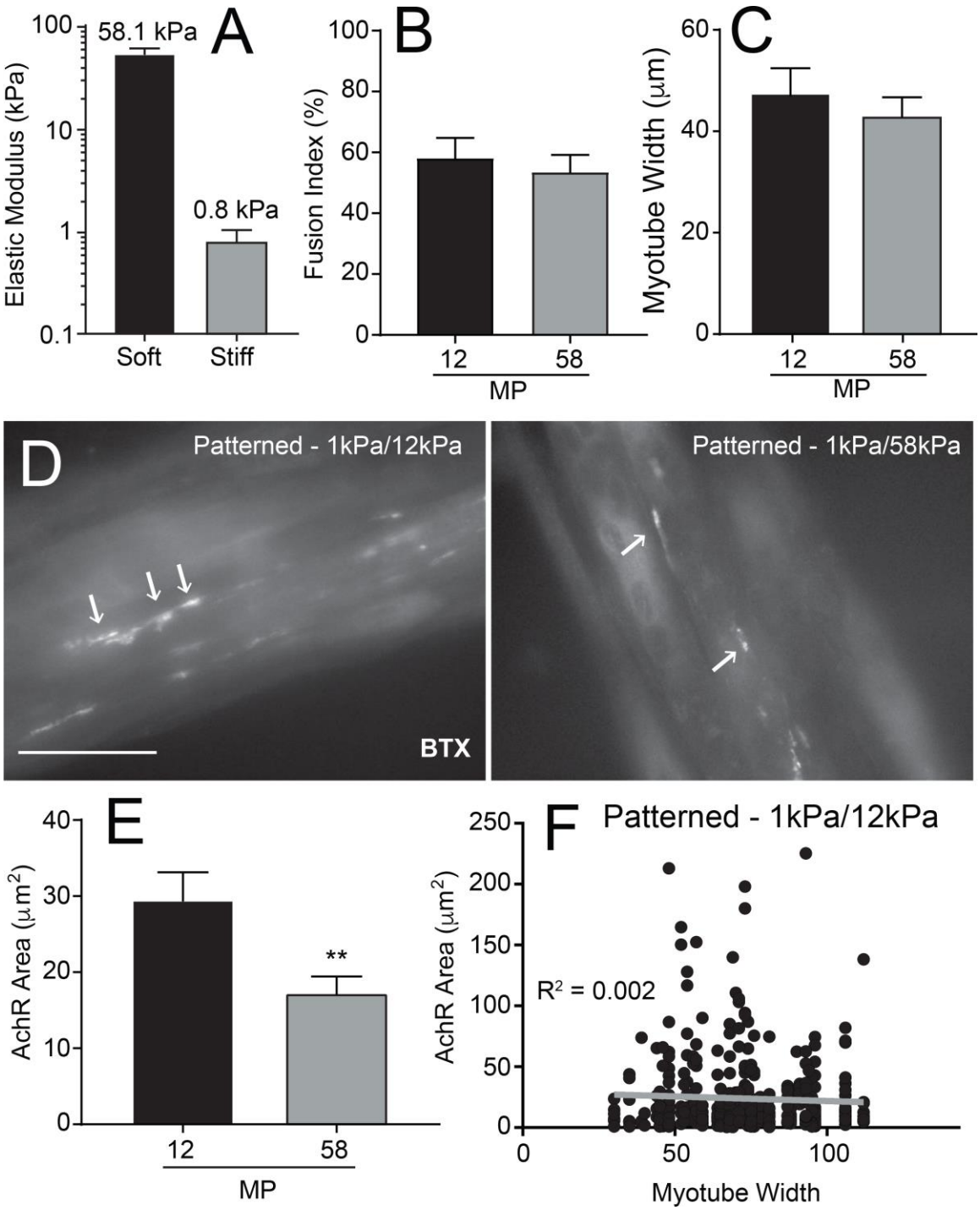

Fig. 7. Substrate Stiffness, But Not Myotube Width, Mediates AchR Cluster Formation on Mechanically Patterned Substrates. (A) Plot of elastic modulus of pathological mechanically patterned hydrogel. Fusion index (B) and myotube width (C) of mouse myotubes cultured on mechanically patterned hydrogels with myogenic (12 kPa) and pathological (58 kPa) stiff regions (n = 25). (D) Representative fluorescent images of AchR clustering on patterned hydrogels. AchR clusters are labeled with α-bungarotoxin (BTX). Scale bar indicates 10 microns. (E) Plot of AchR cluster area on myotubes cultured with agrin treatment on patterned hydrogels. (n = 25) ** $p<0.01$ based on unpaired t-test comparison. (F) Scatter plot of AchR cluster size versus myotube width on mechanically patterned substrates with myogenic (12 kPa) stiff regions (n = 236 AchR clusters).